Research Article

Xizhou Wang, Xianghong Xu*, and Yang Gu

Dynamic response of Voronoi structures with gradient perpendicular to the impact direction

Abstract: Gradient porous structures are extensively studied in impact-resistant structures due to their light weight and high energy absorption. Different from existing studies, this article focuses on novel Voronoi structures with gradient perpendicular to impact direction, and compares their dynamic response with the uniform structure through numerical simulation. It shows that the novel gradient design comprehensively improves the impact resistance of Voronoi structures. Furthermore, density gradient is introduced into the one-dimensional shock model, and the theoretical solution of the plateau stresses at the impact end are compared with the simulation results, which verifies the correctness of the model in this article.

Abbreviations

DOF	degree of freedom
EPPR	elastic perfectly-plastic rigid
FE	finite element
RLHPL	rigid linearly-hardening-plastic locking
RPH	rigid plastic-hardening
RPPL	rigid perfectly-plastic locking
TO	topology optimization

* **Corresponding author: Xianghong Xu,** State Key Laboratory of Nonlinear Mechanics, Institute of Mechanics, Chinese Academy of Sciences, Beijing 100190, China, e-mail: xxh@lnm.imech.ac.cn
Xizhou Wang, Yang Gu: State Key Laboratory of Nonlinear Mechanics, Institute of Mechanics, Chinese Academy of Sciences, Beijing 100190, China; School of Engineering Sciences, University of Chinese Academy of Sciences, Beijing 100049, China

1 Introduction

Honeycomb, animal skeleton, corkwood [1], and other natural porous structures are characterized by lower density and higher plastic deformation capacity than base materials. Thus, porous structures have both light weight and excellent energy absorption performance. At present, biomimetic porous structures have been widely used in impact protection structures, such as foamed aluminum composite armor of armored vehicles, fuselage of large civil airplanes, automotive crash box, landing pads of space capsules, explosion-proof deck of naval vessels, and headstock anti-collision device of high-velocity trains [2–6]. With the rapid development of modern science and technology, higher requirements have been proposed for the impact resistance of materials or structures. On the premise of light weight, researchers have adopted methods such as topology optimization of cell structures [7–9], carbon fiber-reinforced base materials [10,11], and gradient design of cell geometric parameters [12–23], aiming to improve the anti-impact performance of porous structures.

In reported studies on the impact resistance of porous structures, the gradient design of cell geometric parameters is always along the direction of impact. One is layered gradient porous structure [12–16], i.e., the structure is equally divided into finite layers along impact direction, in which cell geometric parameters are uniformly distributed in a layer and are in gradient distribution among different layers. Another is continuous gradient porous structure [17–23], i.e., the cell geometric parameters are in continuous gradient distribution along impact direction. Specifically, if the cell wall thickness decreases or cell size increases along the impact direction, it is called positive gradient; on the contrary, it is called negative gradient.

In terms of numerical simulation and experiment, Ajdari et al. [12] designed two-dimensional regular honeycombs and Voronoi structures with layered gradient in cell wall thickness, and analyzed the deformation and energy absorption characteristics of the gradient

structures under impact compression at different velocities with finite element (FE) method. Zhang et al. [13] designed two-dimensional circle arc porous structures with layered gradient in cell wall thickness, and simulated the crushing response at different impact velocities with FE method. Liu et al. [14] designed three-dimensional metal hollow sphere foams with layered gradient in cell wall thickness, analyzed the stress response and energy absorption characteristics of positive and negative gradient structures at different impact velocities with FE method, and gave the semi-empirical formula for the plateau stress at both ends of the structures. Chen et al. [15] provided layered design for three-dimensional Voronoi foams, and investigated the effect of layered arrangement on structural deformation and energy absorption with FE method. Liang et al. [17] designed continuous gradient two-dimensional Voronoi structures and investigated the effect of the continuous gradient design on the buffering and energy absorption of the structure with FE method. Chen et al. [18] designed two-dimensional Voronoi structures with symmetrical continuous gradient distribution, and simulated the effects of cell porosity gradient, cell wall thickness, cell count, and impact velocity on structural energy absorption with FE method. Duan et al. [20] and Zhao et al. [23] fabricated Voronoi structures with gradient by additive manufacturing technology successfully, and verified the simulation results with experiments.

The gradient design of cell geometric parameters along the impact direction has different effects on the energy absorbed by porous structures with different impact velocities and deformation stages [13–19]. In the plateau stage, the gradient design along the impact direction can improve energy absorption of the porous structure under medium and high-velocity impacts, but the gradient structure has a poor energy absorption under low-velocity impact. In case of high-velocity impact, the energy absorption of positive gradient structure is obviously higher than that of negative gradient structure and uniform structure with the same strain; in case of medium-velocity impact, the positive gradient structure's improvement effect in energy absorption is weakened; in case of low-velocity impact, positive and negative gradient structures under equal strain have nearly the same energy absorption, which is lower than that of the uniform structure. When the nominal strain is 0.5, compared with the uniform structure, the energy absorption of positive gradient structure under high and medium-velocity impacts can be improved by up to about 32 [13] and 26% [12], respectively. Under low-velocity impact, energy absorbed by gradient structure can be up to 34% [12] lower than that of uniform structure. When it comes to the densification strain,

the gradient structure and uniform structure have almost the same energy absorption under any impact velocities [19].

In terms of theoretical research, Reid and Peng [24] proposed a one-dimensional shock model for uniform porous materials, which assumes that the model was in one-dimensional strain state and ignores the effects of deformation and inertia effect in the lateral direction. Based on the one-dimensional shock model and combined with different engineering backgrounds, researchers proposed some stress–strain idealized models for uniform porous materials, such as the rigid perfectly-plastic locking model [24], the elastic perfectly-plastic rigid model [25], the rigid linearly-hardening-plastic locking model [26], and the rigid plastic-hardening model [27]. In addition, Shen et al. [28], Karagiozova and Alves [29], Liu et al. [30], Yang et al. [31], Liu et al. [32], and Ding et al. [33] developed the one-dimensional shock model to study the dynamic response of gradient porous structures under uniaxial impact compression. For porous structures with layered and continuous gradients along the impact direction, Liang et al. [17] and Zhang et al. [16] developed corresponding theoretical models, respectively, and verified them with numerical analysis.

This article is organized as follows. In Section 2, Voronoi structures with gradient perpendicular to impact direction were designed. In Section 3, the effect of the gradient design on the impact compression performance of the Voronoi structure was analyzed with FE method. In Section 4, design of density gradient perpendicular to impact direction was introduced to further develop the one-dimensional shock model for gradient porous structures. Section 5 ends the article with some conclusions.

2 Methods and modeling

2.1 Gradient Voronoi structures

Gradient Voronoi structures are generated by combining the spreading circle method [34] and gradient grid method [35] (Figure 1).

Step 1: Determine the number of grids per layer.

The rectangular region of length L_1 and height L_2 is divided into I layers, and the ith layer is equally divided into J_i grids,

$$J_i = \text{INT}\left[\frac{N + \sum_{k=1}^{I} 0.55a\left(k - \frac{I+1}{2}\right)^2}{I} - 0.55a\left(i - \frac{I+1}{2}\right)^2\right] \quad (1)$$
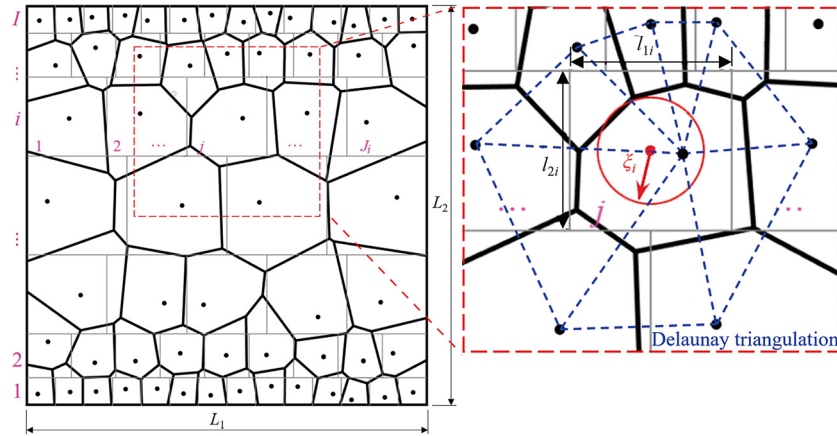
Figure 1: Schematic diagram of gradient Voronoi model generated by gradient grid and spreading circle methods. The length and height of the model are L_1 and L_2, respectively; the thin solid lines and the thick solid lines represent cell edges and the grids, respectively, the dashed lines represent the Delaunay triangle network, and the dots represent the cell cores; the number of grid layers is I, J_i, ξ_i, l_{1i}, and l_{2i} represent the layer-cell-number, the radius of spreading circle, grid length, and height of the ith layer, respectively.

where INT refers to the rounding function, N refers to the total number of cells, and a refers to the gradient coefficient along the direction of height. Step 1 determines the gradient of the generated structure by controlling the value of a.

Step 2: Calculate the length–height ratio.

In the ith layer, the grid length $l_{1i} = L_1/J_i$, the grid height l_{2i} shall satisfy that

$$\frac{l_{1i}}{l_{2i}} = \frac{\sum_{i=1}^{I}(L_1/J_i)}{L_2}. \tag{2}$$

Step 2 ensures that all grids have the same length–height ratio.

Step 3: Generate cell cores.

In the grid of the ith layer, the spreading circle is made with grid centroid as center and ξ_i as radius, and ξ_i shall satisfy that,

$$\xi_i = \lambda\min(l_{1i}, l_{2i}), \tag{3}$$

where λ refers to the radius coefficient of the spreading circle and $0 \le \lambda \le 1$. In each spreading circle, a cell core is chosen randomly. Step 3 determines the irregularity of the generated structure. The smaller the value of λ, the smaller the differences in shape and size of the cells within the same layer.

Step 4: Generate Voronoi model.

Delaunay triangulation network is constructed based on all generated cell cores. For any cell core, a Voronoi polygon (i.e., a cell) can be obtained by connecting the circumcenter of all adjacent triangles, and the common edges of adjacent cells are not connected repeatedly. A solid Voronoi model can be obtained by translating the

edges of all generated Voronoi polygons in-plane to ensure that all cell walls have the same thickness b. The relative density of the model can be obtained by getting the total area of all cell walls to be divided by the area of the two-dimensional region. When calculating the total area of cell walls, if the cell wall thickness b is far below its length, the overlapped area between cell walls is a high-order infinitesimal and thus can be ignored. When the model relative density, length L_1 and height L_2, total number of cells N, number of grid layers I, and gradient coefficient a are given, then layer-cell-number J_i, grid sizes l_{1i} and l_{2i} ($i = 1,2,...I$), and the cell wall thickness b will be uniquely determined. Step 4 generates Voronoi model according to the cell cores generated in step 3, and control the relative density of the generated structure by changing the cell wall thickness b.

Figure 2a gives the distribution curves of layer-cell-number J_i versus grid layers. The relative density of Voronoi model is 5.5%, length $L_1 = 20$ mm, height $L_2 = 20$ mm, out-of-plane thickness $L_3 = 1$ mm, total number of cells $N = 900 \pm 5$, number of grid layers $I = 29$, the radius coefficient of the spreading circle $\lambda = 1/3$, and gradient coefficient $a = 0$, 0.25, 0.35, −0.4, −0.6, respectively. The 15th layer is the central layer, and J_i is symmetric about it, and the distribution of J_i along the direction of height is uniquely determined by the gradient coefficient a. In order to avoid the appearance of severely distorted cells, the value of a is between −0.6 and 0.35. The layer-density is defined as the sum of the cell wall volume of each layer multiplied by the density of base materials, and then divided by the total volume of the grids of the layer, where the volume of cell walls between
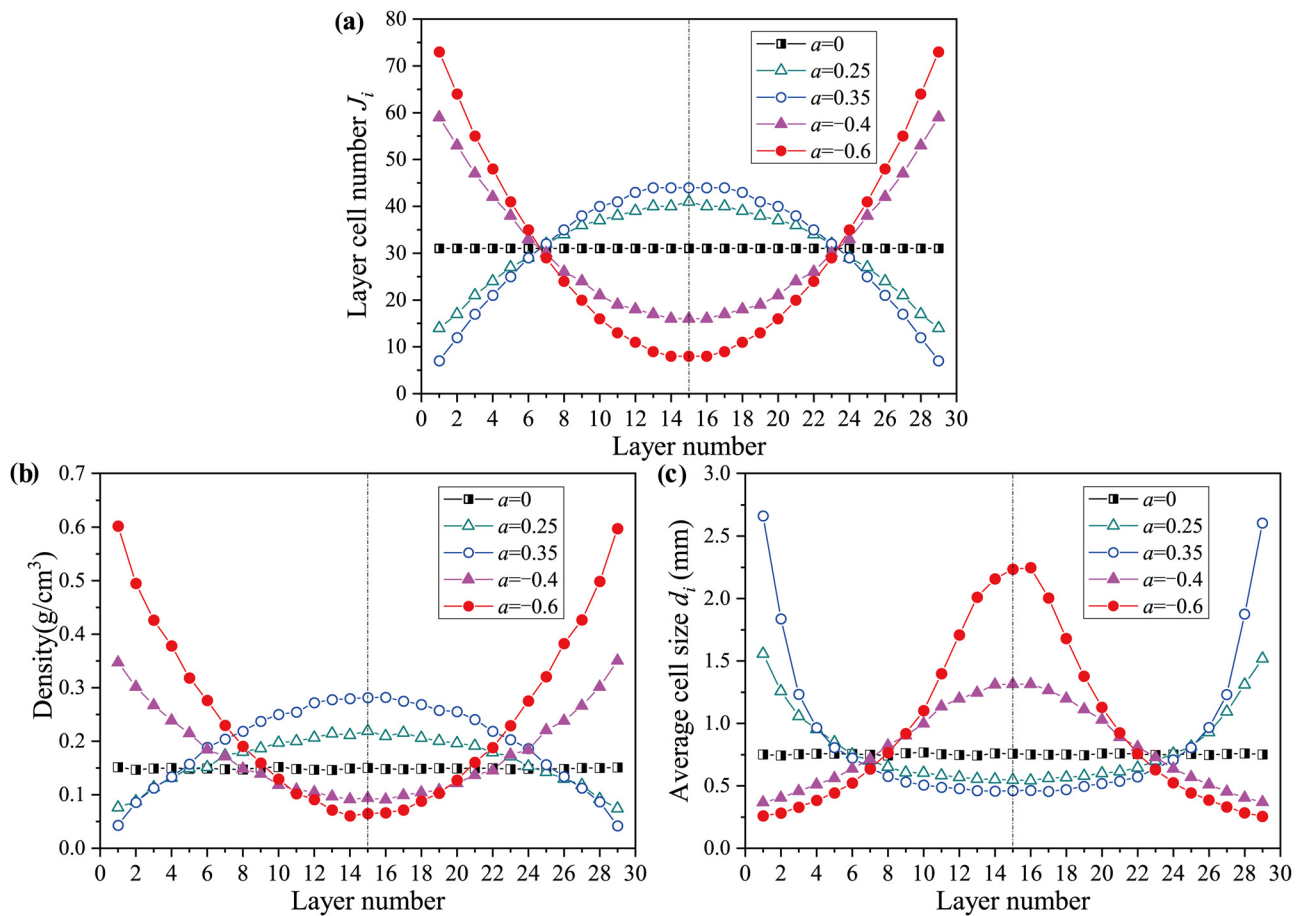
Figure 2: Distribution curve of the (a) layer-cell-number J_i, (b) layer-density, and (c) layer-cell-size versus grid layers. The total number of cells $N = 900 \pm 5$; number of grid layers $I = 29$; the radius coefficient of the spreading circle $\lambda = 1/3$. All Voronoi models have a relative density of 5.5%.

two layers is equally shared (Figure 2b). The layer-cell-size is defined as the average diameter of equal-area circles of all polygon cells in each layer (Figure 2c).

Figure 3 shows the generated Voronoi models. When $a = 0$, J_i is a constant, the layer-cell-size and layer-density of each layer are nearly equal, which is known as a uniform model (Figure 3a); when $a > 0$, the layer-cell-number on the upper and lower edges is lower than that in the center of the model, while the layer-cell-size and layer-density increase from the center to the edges, which is known as a positive gradient model (Figure 3b and c); when $a < 0$, the layer-cell-number on the upper and lower edges is higher than that in the center of the model, while the layer-cell-size and layer-density decrease from the center to the edges, which is known as a negative gradient model (Figure 3d and e). It can be seen that the greater the absolute value of a, the greater the change gradient of layer-cell-number, and the larger the varying gradient of layer-cell-size and layer-density.

2.2 FE model

The FE software Abaqus/Explicit was used to numerically simulate the uniaxial impact compression process of Voronoi models. The base material of the model is Al-5052-H39 [36], with a density of 2,750 kg·m^{-3} and the bilinear kinematic hardening elastoplastic constitutive model, its elastic modulus is 68.97 GPa, the Poisson's ratio is 0.32, the yield stress is 282 MPa, the post-yield modulus is 0.69 GPa, and the plastic strain limit is 0.287. When the strain exceeds this value, the stress will remain unchanged at 480 MPa.

Figure 3a is the schematic diagram of the Voronoi model under uniaxial impact compression. The support rigid and impact rigid are set on the left and right sides of the model, respectively, of which the support rigid is fixed, while the impact rigid is applied with a constant impact velocity v along the x-axis. The impact velocities are 5, 25, and 150 m·s^{-1}, respectively. All FE models of
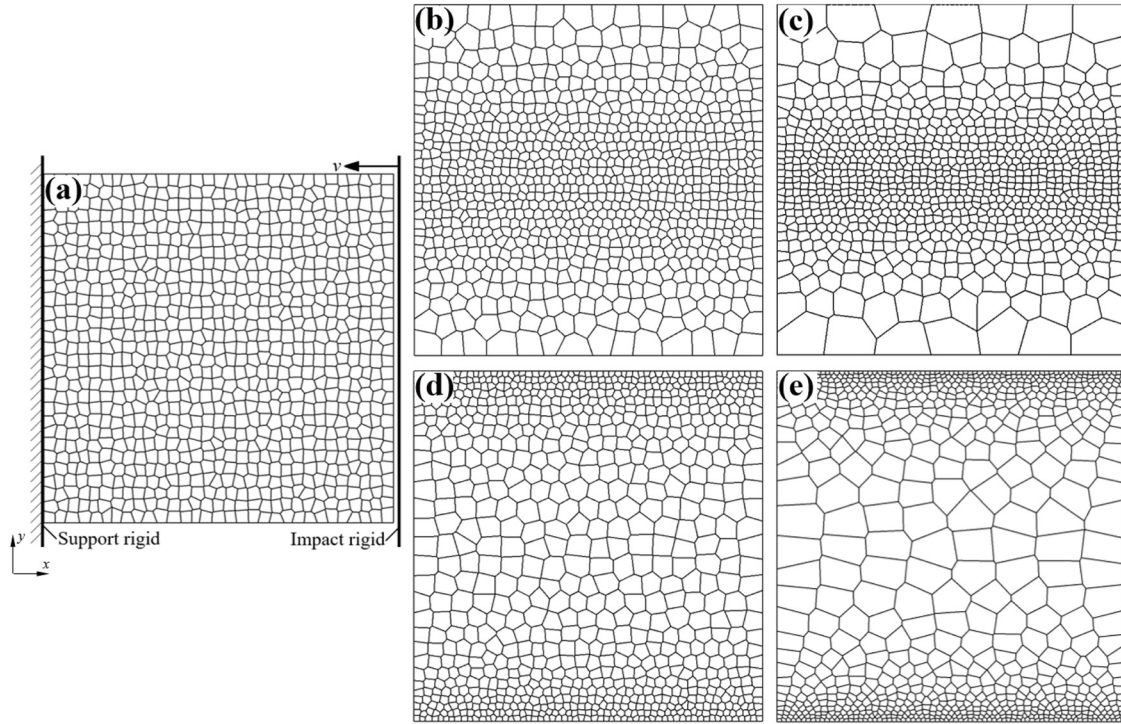
Figure 3: Voronoi models and the schematic diagram of uniaxial impact compression. Gradient coefficient a = (a) 0, (b) 0.25, (c) 0.35, (d) −0.4, and (e) −0.6.

Voronoi structures are meshed by S4R shell element. The uniaxial impact compression of Voronoi model is a kind of plane strain problem, which constrains the out-of-plane rotation and displacement of all nodes in the model, with three degrees of freedom per node. The displacement along the y-axis direction at the intersection of the cell walls on the upper and lower boundaries of the model is constrained. In addition, self-contact is set between all cell walls and between cell walls and the rigid plates, with a friction coefficient of 0.02.

3 Results and discussion

3.1 Nominal stress–strain curve and plateau stress

Figure 4a gives the nominal stress–strain curves at the impact end of Voronoi structures under uniaxial impact compression. Specifically, nominal stress is obtained by getting the support reaction force of the right rigid plate to be divided by the contact area L_2L_3, nominal strain is obtained by dividing the compression of the model along the length by L_1. Similarly, divide the support reaction

force of the left rigid plate by L_2L_3 to obtain the nominal stress at the support end of the model (Figure 4b). Therefore, similar to the uniform structure, the nominal stress–strain curve of the gradient structure is divided into three stages, i.e., linear elasticity stage, plateau stage, and densification stage [37]. The initial stage of impact compression is the linear elasticity stage, during which the nominal stress increases linearly with nominal strain. Later, it is the plateau stage, during which the nominal stress stabilizes at a certain level and no longer increases with nominal strain. Finally, it is the densification stage, during which the nominal stress–strain curve rises sharply.

The plateau stress is defined as the average value of the nominal stress in the plateau stage, the plateau stresses of the support end and the impact end are denoted as σ_0 and σ^*, respectively. In view of the nominal stress–strain curves under middle or low-velocity impact compressions (the thick solid line in Figure 5), the onset point of plateau stage A corresponds to the point where the stress tends to be stable; the end point of plateau stage B corresponds to the onset point of the densification stage, and the strain of the point is denoted as ε_{cd}. In the plateau stage, the stress is stable, and the energy absorption efficiency $\left(\int_0^\varepsilon \sigma(\varepsilon)\mathrm{d}\varepsilon / \sigma(\varepsilon)\right)$ increases with the nominal
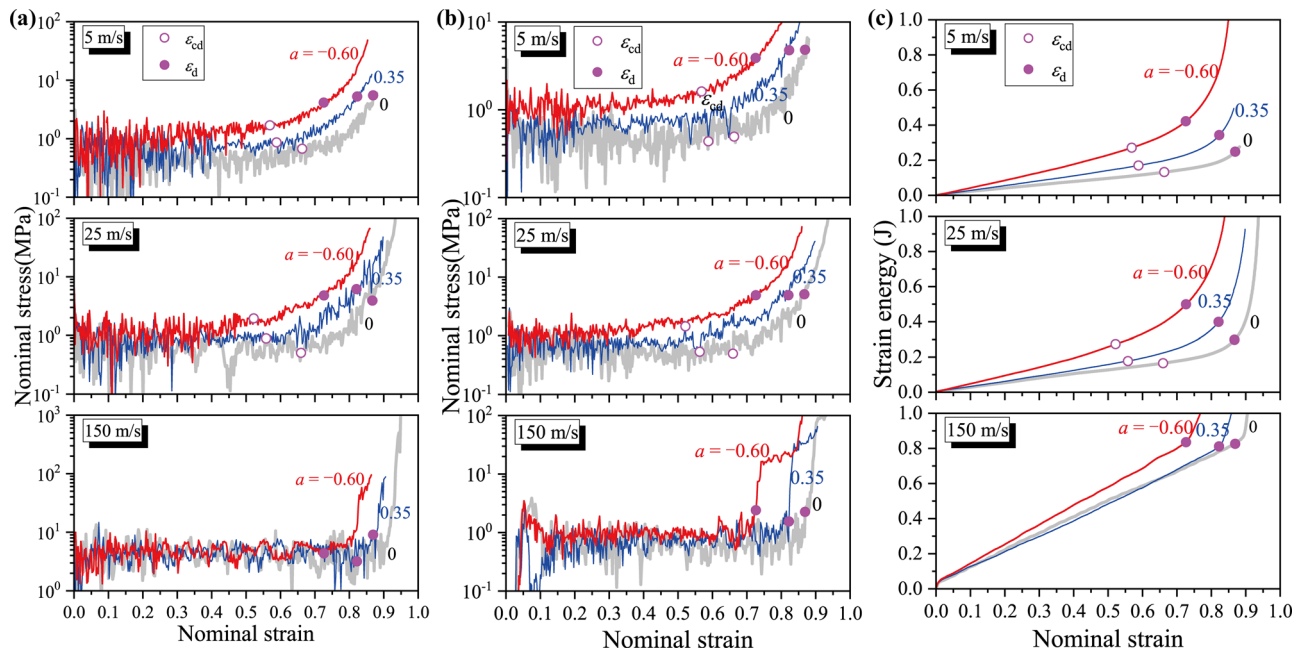
Figure 4: Curves of (a) impact end stress, (b) support end stress, and (c) strain energy of the Voronoi models under uniaxial impact compression.
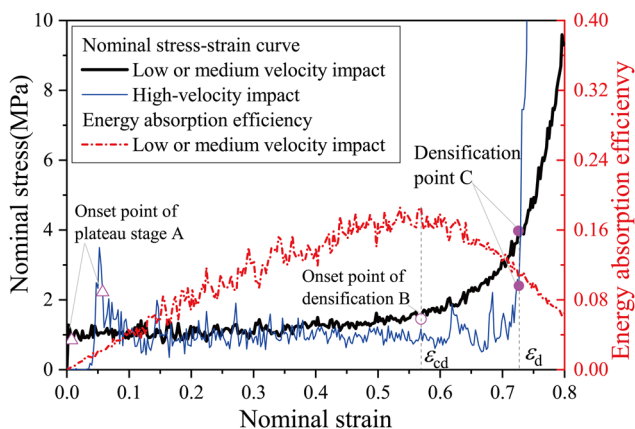
Figure 5: Characteristic strain points of the Voronoi under impact compression: A, B, and C represent the onset point of plateau stage, the onset point of densification stage, and the densification point, respectively.

strain; in the densification stage, the stress increases, while the energy absorption efficiency decreases [38] (the dotted line in Figure 5). Therefore, the turning point of the energy absorption efficiency curve corresponds to Point B. After entering the densification stage, cells are compressed to fully collapse gradually. When the structure is fully dense, material of cell walls is compressed [37], and the point is called as densification point which corresponds to densification strain ε_d. In view of high-velocity impact compression, cells collapse layer by layer from the impact end

Voronoi structure is fully dense at the end of plateau stage. Therefore, the values of ε_{cd} and ε_d are equal at high-velocity impact, i.e., the end point of plateau stage B and the densification point C are the same point, which can be determined by the change in trend of the nominal stress–strain curve (the thin solid line in Figure 5). For the same Voronoi structure, the nominal strain is the same when it is compressed to be fully dense, so ε_d is unrelated to impact velocity.

As shown in Figure 6a, the plateau stress of the support end σ_0 is mainly affected by the characteristics of the structure itself during impact compression. In the plateau stage, the velocity of materials at the support end is almost 0 and the deformation is small, the inertia effect can be ignored, in which case the difference in σ_0 of the same structure is small at different impact velocities. For the same impact velocity, the larger the varying gradient of layer-cell-size, the higher the σ_0 of the gradient structure, which can reach up to 2.4 times of that of uniform structure.

The plateau stress of the impact end σ^* is affected by the characteristics of the structure itself and the impact velocity. Due to the inertia effect, for the same structure, the greater the impact velocity, the higher the value of σ^*. Under low-velocity impact, interior of Voronoi structure is approximately in the state of stress equilibrium, and σ^* is mainly affected by the characteristics of the structure itself, which is almost equal to σ_0; under
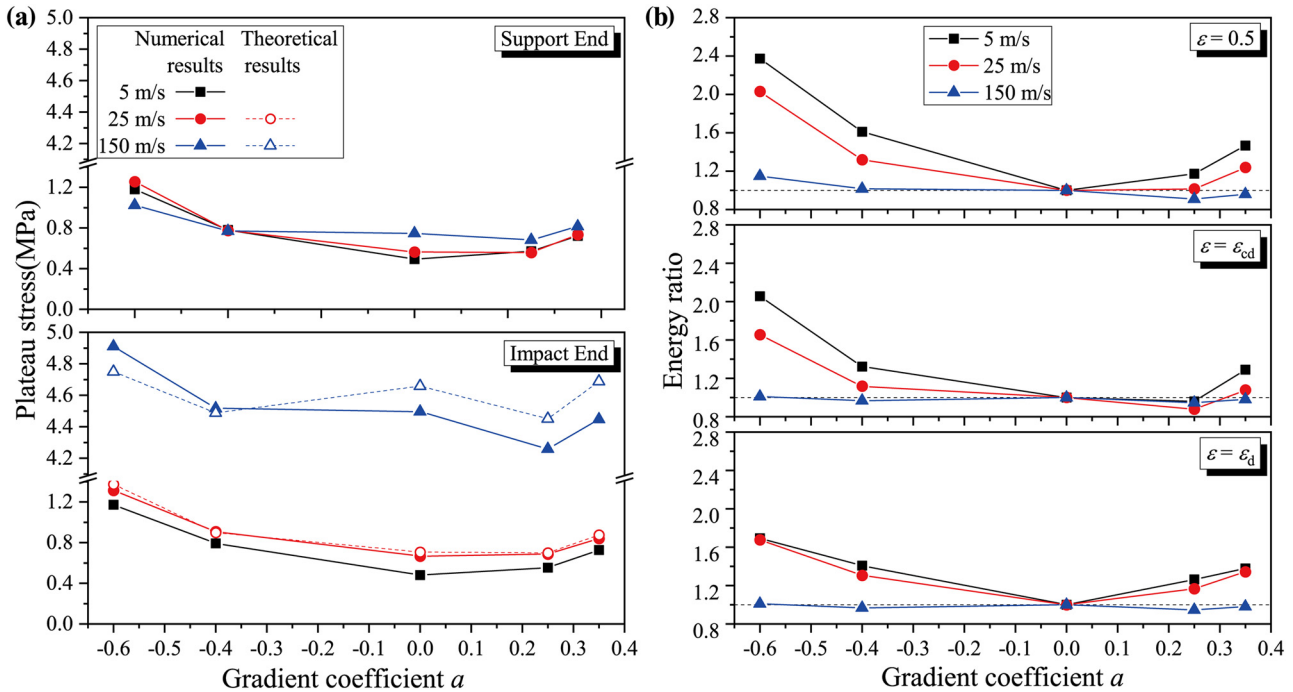
Figure 6: Curves of (a) the plateau stress and (b) energy ratio versus gradient coefficient.

medium-velocity impact, σ^* slightly increases than that under low-velocity impact due to the joint action of the characteristics of the structure itself and the inertia effect; under high-velocity impact, σ^* is mainly affected by the inertia effect, which is several times of that under low-velocity impact. For the same impact velocity, the larger the varying gradient of layer-cell-size, the higher the σ^* of the gradient structure. Under low-velocity impact, the maximum σ^* of the gradient structure is about 2.4 times of that in the uniform structure; as the impact velocity increases, the effect of the characteristics of the structure itself on σ^* decreases. Under high-velocity impact, the maximum σ^* of the gradient structure is only 1.1 times that of the uniform structure.
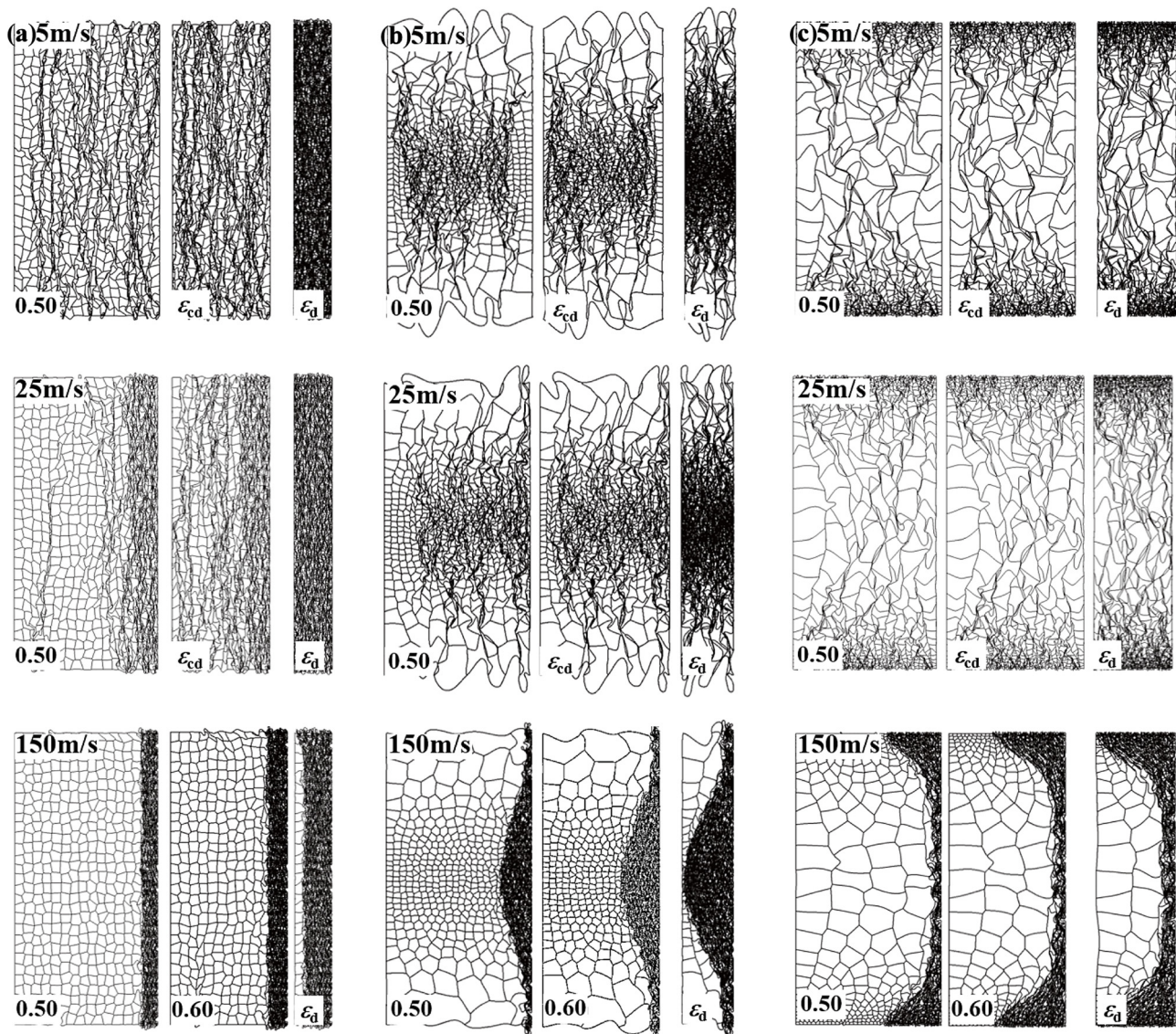
3.2 Deformation mode

Figure 7 gives the deformation modes of Voronoi structures under uniaxial impact compression. When the impact velocity is $5\,\mathrm{m\cdot s^{-1}}$, the internal structure is in the state of stress equilibrium, cells collapse randomly and produce crush bands, and the macroscopical deformation of the structure is homogeneous, which is a quasi-static mode [39] under low-velocity impact. When the impact velocity is $25\,\mathrm{m\cdot s^{-1}}$, the structural deformation is affected by the inertia effect, crush bands are mostly concentrated

at the impact end and they are even more densely distributed in the region with a higher layer-density in the gradient structure, which is a transition mode [39] under medium-velocity impact. When the impact velocity is $150\,\mathrm{m\cdot s^{-1}}$, the inertia effect plays a leading role in structural deformation, and cells collapse sequentially from the impact end, which is a dynamic mode [39] under high-velocity impact. At this time, the deformation of the gradient structure is obviously different from that of the uniform structure. The layer-densities in the uniform structure are almost equal, the shock wave propagates at the same velocity at different ordinates, and the shock wave front lies on a straight line. In regions with a higher layer-density in the gradient structure, the shock wave has a faster propagation velocity, and the shock wave front is parabolic, which explains why the onset strain of densification ε_{cd} and the densification strain ε_d of the gradient structure are lower than those of the uniform structure.

3.3 Energy absorption

Under impact load, the energy absorbed by Voronoi structure is mainly transformed into strain energy (elastic strain energy and plastic strain energy) stored in the structure. Figure 4c gives the curve of the strain energy

Figure 7: Deformation modes of Voronoi structures. Impact velocities are 5, 25, and 150 m·s^{-1}, respectively. Gradient coefficient a = (a) 0, (b) 0.35, and (c) −0.6.

stored in the model changing with the nominal strain ε. When $\varepsilon < \varepsilon_{cd}$, the strain energy stored in the structure linearly increases with the nominal strain; when $\varepsilon_{cd} \leq \varepsilon < \varepsilon_d$, the structure is compressed to be dense gradually, and the slope of the strain energy curve increases gradually; when $\varepsilon \geq \varepsilon_d$, the structure has been compressed to be fully dense and loses its buffering capacity, the strain energy curve rises sharply.

Under the same impact velocity and characteristic strain point, the ratio of strain energy stored in gradient structure to that in uniform structure is defined as energy ratio. Figure 6b gives the curve for the energy ratios of three characteristic strain points changing with gradient coefficient at different impact velocities. Voronoi structures have the best energy absorption effect in the plateau stage, stress at both ends of the structure are relatively stable, and the values of ε_{cd} in all models is greater than 0.5, so 0.5 is taken as the first characteristic strain point, at which the energy absorption performance of different structures under equal strain in the plateau stage are compared. It can be found that the larger the varying gradient of layer-cell-size, the higher the energy ratio under the same impact velocity. The higher the impact velocity, the lower the energy ratio of the same gradient structure, and less effect of the gradient coefficient on the energy ratio. Under low-velocity impact, the energy ratio can reach up to 2.4; under high-velocity impact, the energy ratio can reach up to 1.1 only. The second characteristic

strain point adopts ε_{cd}, which corresponds to the end of the plateau stage and the onset of the densification stage of the Voronoi structure, where stress at both ends begins to rise, while the buffering capacity starts to drop, and the strain energy at the time of ε_{cd} can reflect the structure's energy absorption characteristics with effective buffering and protective function. ε_d is adopted as the third characteristic strain, which corresponds to the Voronoi structure has been compressed to be fully dense, and the stress at both ends begins to rise sharply. The strain energy at the time of ε_d can reflect the maximum energy absorption capacity of the moment before the structure loses buffering capacity. The changing law of energy ratio with gradient coefficient and impact velocity at ε_{cd} and ε_d is similar to that at the characteristic strain point of 0.5. The shock wave first reaches the support end at the layer with the highest layer-density, so the ε_{cd} of the gradient structure is smaller than that of the uniform structure; similarly, layer with the maximum layer-density in the gradient structure is compressed to be fully dense earlier, and thus the ε_d is also smaller than that of the uniform structure. In addition, the larger the varying gradient of layer-cell-size, the smaller the values of ε_{cd} and ε_d. Compared with the situation under equal strain of 0.5, the energy ratios of the same gradient structure at the strain of ε_{cd} and ε_d decrease successively. At the same time, the difference in the energy ratio caused by the change of layer-cell-size becomes smaller, and the higher the impact velocity, the smaller the difference. Under low-velocity impact, the energy ratio at the time of ε_{cd} reaches the maximum of about 2.1, and

that at the strain of ε_d reaches the maximum of about 1.7; while under high-velocity impact, the energy ratio at the strain of ε_{cd} and ε_d is about 1.

According to the statistical analysis of the strain energy stored in the structure at the equal strain in the plateau stage, effective protection stage and the moment of full densification, the gradient design perpendicular to impact direction can increase the energy absorbed by Voronoi structure under uniaxial impact compression, and improve its anti-impact performance comprehensively. At the same impact velocity, the larger the varying gradient of layer-cell-size, the more energy absorption of the gradient structure. Specifically, the structure whose gradient coefficient is –0.6 has the best energy absorption effect. Under low-velocity impact, the energy absorptions at the nominal strain of 0.5, ε_{cd} and ε_d are 2.4, 2.1, and 1.7 times those of the uniform structure, respectively. To sum up, as the impact velocity increases, the effect of the gradient design on structural energy absorption decreases. At the impact velocity of 150 m·s^{-1}, the energy absorption of the gradient structure is nearly the same as that of the uniform structure.

3.4 Mechanism analysis of gradient design on energy absorption

Figure 8 gives the curve for the average Mises stress and total strain energy of each layer in the Voronoi model at
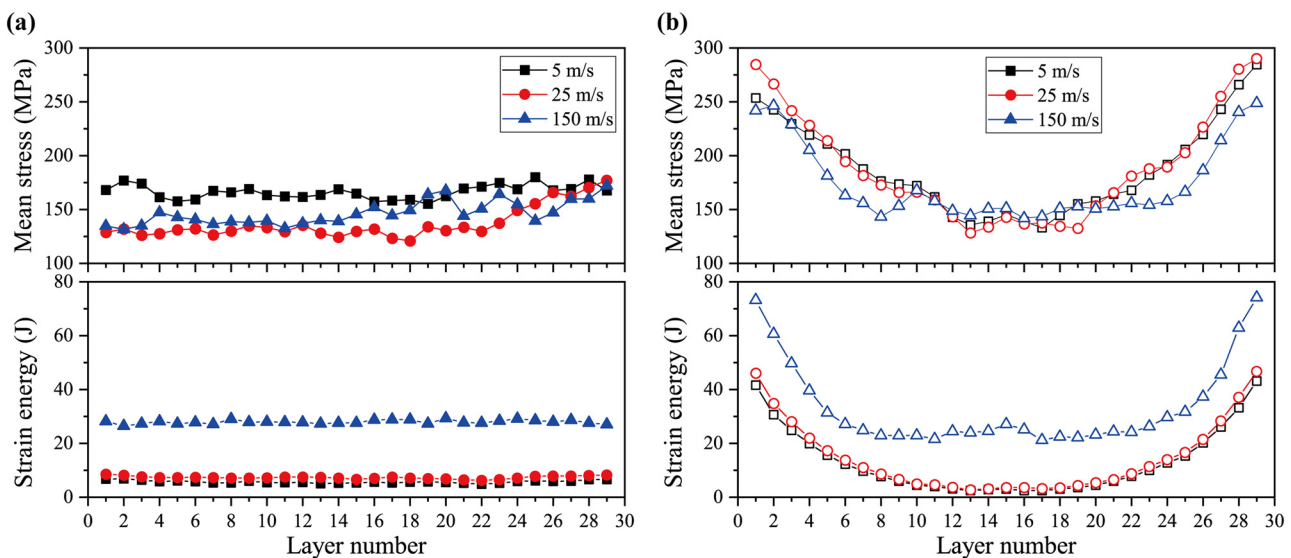

Figure 8: Curves of the average Mises stress and total strain energy versus grid layers. Gradient coefficient a = (a) 0, and (b) –0.6. Nominal strain ε = 0.5.

the nominal strain of 0.5. In the uniform structure, the average Mises stress of each layer is similar, and the stored strain energy is nearly the same (Figure 8a). In the gradient structure, the smaller the layer-cell-size in the layer, the higher the layer-density, and higher the average Mises stress and stored strain energy (Figure 8b). Under the same relative density and impact velocity, the strain energy stored in the middle layer of the negative gradient model is equivalent to that of the uniform structure, while that stored in other layers is higher than that in the corresponding layers of the uniform structure, which makes the strain energy stored in the gradient structure higher than that in the uniform structure.

Specifically, for the negative gradient model whose a is −0.6, the average Mises stress in the middle layer is about 0.9 times that in the same layer of the uniform structure, but that in the marginal layer can reach the maximum of 2 times that of the middle layer, much higher than that of the uniform structure. Similarly, the strain energy stored in the middle layer under low-velocity impact is about 0.6 times that of the uniform structure, while that stored in the marginal layer is 14.1 times that of the middle layer, which is 6.6 times that of the same layer in the uniform structure. With the increase of the impact velocity, the difference in the energy stored between the same layer of the gradient structure and uniform structure becomes smaller, the difference in the energy stored between the marginal layer and the middle layer of the negative gradient structure becomes smaller, the effect of the gradient design on energy absorbed by Voronoi structure decreases. Under high-velocity impact, for the negative gradient model whose a is −0.6, the strain energy stored in the middle layer is nearly the same as that stored in the corresponding layer of the uniform structure, and the strain energy stored in the marginal layer is about 2.7 times that stored in the middle layer.

4 One-dimensional shock model for gradient Voronoi structure

Under low-velocity impact, the internal structure is in the state of stress equilibrium, and the plateau stresses on both ends are almost equal. Figure 9 gives the one-dimensional shock model for the gradient Voronoi structure under medium and high-velocity impacts. Assuming that the specimen is in the state of one-dimensional strain, the velocity of the area not swept by shock wave
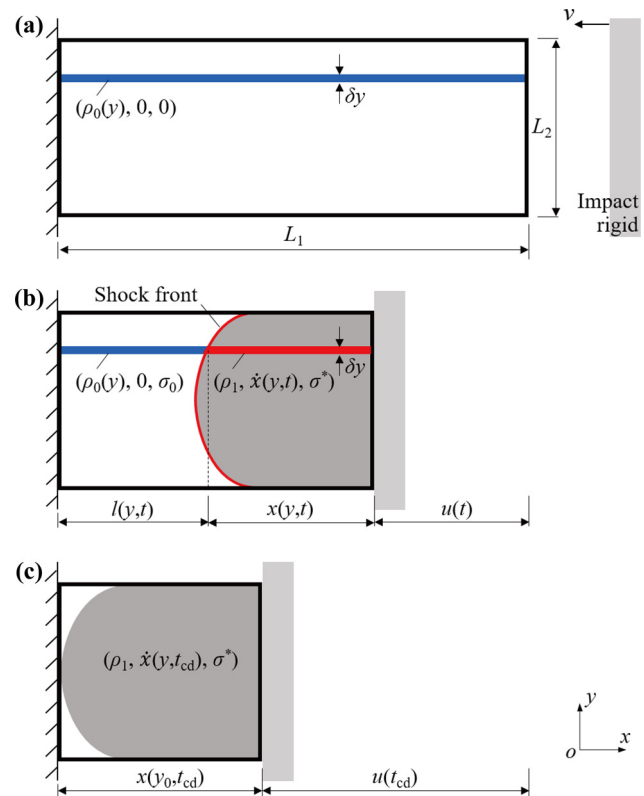
Figure 9: One-dimensional shock model for gradient Voronoi structure: (a) uniaxial impact compression model, (b) at time t, and (c) at time t_{cd}.

is 0, and the density remains unchanged. The velocity of the area swept by shock wave is the same as the impact velocity, and the density after compression is uniform at each point. In the specimen with length L_1, height L_2, and out-of-plane thickness L_3, the density is in gradient distribution along the direction of y-axis, and the initial density of the micro-element δy at any height y is denoted as $\rho_0(y)$. The support rigid is on the left side of the specimen, and the impact rigid with a constant velocity v is on the right side of the specimen (Figure 9a). At time 0, the impact rigid contacts the right side surface of the specimen, and the compression process begins. At time t (Figure 9b), the displacement of the right side surface of the specimen along the direction of x-axis is $u(t)$. The left side of the micro-element δy is the area not swept by shock wave, its length is $l(y,t)$, there is only a small elastic deformation, the initial density remains unchanged, the velocity at each point is 0, and the normal stress along the direction of x-axis is σ_0, i.e., the plateau stress at support end. The right side of the micro-element δy is the area swept by shock wave, its length is $x(y,t)$, and cells are collapsed after compression. Assuming that the density at each point is uniform, the density after compression

is ρ_1, the velocity is $x(y,t)$, and the normal stress along the direction of x-axis is σ^*, i.e., the plateau stress at impact end. According to the geometrical relationship:

$$L_1 = l(y, t) + x(y, t) + u(t), \tag{4}$$

take the derivative of both sides with respect to time t,

$$\dot{l}(y, t) + \dot{x}(y, t) = -\dot{u}(t), \tag{5}$$

where $\dot{u}(t) = v$. According to the principle of mass conservation, the mass of the area swept by the shock wave at the micro-element δy remains unchanged during compression,

$$\rho_1 x(y, t)\delta y = \rho_0(y)[x(y, t) + u(t)]\delta y, \tag{6}$$

derivation of both sides to t, then the shock wave propagation velocity,

$$\dot{x}(y, t) = \frac{\rho_0(y)}{\rho_1 - \rho_0(y)}v. \tag{7}$$

Obviously, the propagation velocity of the shock wave in the micro-element δy is positively correlated with its initial density $\rho_0(y)$. The gradient structure has different initial densities at different heights y, and then it has different propagation velocities of shock wave, in which case the wave front of the gradient structure is parabolic. According to the principle of momentum conservation,

$$(\sigma^* - \sigma_0)L_2 L_3 \delta t = v\delta m, \tag{8}$$

where δt is the time micro-element, δm is the mass of the area swept by the shock wave within the time of δt, and

$$\delta m = \int_0^{L_2} \rho_1 L_3 \dot{x}(y, t)\delta t \, dy. \tag{9}$$

Substituting equation (9) into equation (8),

$$\sigma^* = \sigma_0 + \frac{\rho_1 v}{L_2} \int_0^{L_2} \dot{x}(y, t) \, dy. \tag{10}$$

When $y = y_0$, the initial density $\rho_0(y)$ reaches the maximum, and the propagation velocity of shock wave hits the peak. At time t_{cd} (Figure 9c), the shock wave reaches the support end, and the plateau stage ends, corresponding to the onset strain of densification ε_{cd}, and equation (7) can be expressed as:

$$L_1 = x(y_0, t_{cd}) + u(t_{cd}), \tag{11}$$

and $u(t_{cd}) = L_1\varepsilon_{cd}$, substituting equation (11) into equation (6),

$$\rho_1 = \frac{\rho_0(y_0)}{1 - \varepsilon_{cd}}. \tag{12}$$

Substituting equations (7) and (12) into equation (10), the plateau stress at the impact end in the gradient Voronoi structure can be expressed as:

$$\sigma^* = \sigma_0 + \frac{\rho_0(y_0)v^2}{L_2} \int_0^{L_2} \frac{\rho_0(y)}{\rho_0(y_0) - (1 - \varepsilon_{cd})\rho_0(y)} \, dy. \tag{13}$$

As for the uniform structure, $\rho_0(y)$ in the model is a constant, denoted as ρ_0, equation (13) can be simplified as $\sigma^* = \sigma_0 + \rho_0 v^2/\varepsilon_{cd}$ [24].

According to equation (12), density of the dense area swept by shock wave ρ_1 in different gradient structures can be obtained (Figure 10). At the same velocity, the larger the varying gradient of layer-cell-size, the greater the ρ_1 value of the gradient structure, the more compact the structure under compression, and higher the energy absorption. Figure 6a gives the theoretical solution to the plateau stress at the impact end at medium and high velocities obtained according to equation (13). It is found that the maximum relative difference between the theoretical solution result and the numerical simulation result is about 5.7%, showing high consistency and verifying the correctness of the theoretical analysis in this article.

5 Conclusions

In this work, we have designed Voronoi structures with gradient perpendicular to impact direction, and their dynamic responses under uniaxial impact compression were studied by numerical simulation methods, and the corresponding one-dimensional shock model was proposed. Comparing the theoretical calculation with the
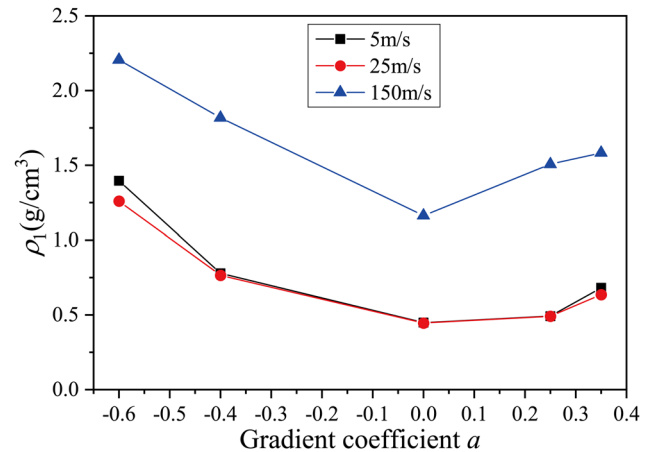

Figure 10: Density of the dense area swept by shock wave ρ_1.

simulation results, the following conclusions can be obtained:

(1) The gradient design perpendicular to impact direction can comprehensively improve the energy absorbed by Voronoi structure, and it is affected by the cell size gradient and impact velocity. At the same impact velocity, the larger the varying gradient of layer-cell-size, the more the energy absorbed by the gradient structure. As the impact velocity increases, the effect of gradient design on the energy absorption of the Voronoi structure decreases.

(2) The gradient distribution of layer-cell-size changes the impact resistance of the Voronoi structure. The layer with a smaller layer-cell-size is denser and bears a higher load, and its stored strain energy is much higher than that of the corresponding layer in the uniform structure, thereby increasing the energy absorbed by the gradient structure. As the impact velocity increases, the strain energy stored in cells increases, the difference between the gradient structure and the corresponding layer in the uniform structure decreases, and the effect of the gradient design on energy absorbed by Voronoi structure decreases.

(3) The one-dimensional shock model for the gradient Voronoi structure in this article is proposed by introducing density gradient perpendicular to the impact direction. Theoretical analysis shows that propagation velocity of the shock wave in the gradient structure is positively correlated with the initial density of cells. The larger the varying gradient of layer-cell-size, the greater the density of the dense area swept by shock wave, the more compact the structure under compression, and more the energy absorbed by gradient Voronoi structure. Through calculation, the theoretical solution of the plateau stress at the impact end is in good agreement with the numerical simulation result, which verifies the correctness of the theoretical model in this article.

Author contributions: Xizhou Wang: writing – original draft, writing – review and editing, investigation, methodology, formal analysis; Xianghong Xu: writing – review and editing, methodology, visualization, project administration, supervision; Yang Gu: methodology, formal analysis.

Conflict of interest: Authors state no conflict of interest.

Data availability statement: The data of these findings cannot be shared at this time as the data also forms part of an ongoing study.

References

[1] Delucia, M., A. Catapano, M. Montemurro, and J. Pailhés. A stochastic approach for predicting the temperature-dependent elastic properties of cork-based composites. *Mechanics of Materials*, Vol. 145, 2020, id. 103399.

[2] Bertolino, G. and M. Montemurro. Two-scale topology optimisation of cellular materials under mixed boundary conditions. *International Journal of Mechanical Sciences*, Vol. 216, 2022, id. 106961.

[3] Gama, B. A., T. A. Bogetti, B. K. Fink, C. J. Yu, T. D. Claar, H. H. Eifert, et al. Aluminum foam integral armor: a new dimension in armor design. *Composite Structures*, Vol. 52, 2001, pp. 381–395.

[4] Betts, C. Benefits of metal foams and developments in modelling techniques to assess their materials behaviour: a review. *Materials Science and Technology*, Vol. 28, 2012, pp. 129–143.

[5] Cheon, S. S. and S. A. Megu. Crush behavior of metallic foams for passenger car design. *International Journal of Automotive Technology*, Vol. 5, 2004, pp. 47–53.

[6] Banhart, J. Manufacture, characterisation and application of cellular metals and metal foams. *Progress in Materials Science*, Vol. 46, 2001, pp. 559–632.

[7] Bauer, J., S. Hengsbach, I. Tesari, R. Schwaiger, and O. Kraft. High-strength cellular ceramic composites with 3D micro-architecture. *Proceedings of the National Academy of Sciences*, Vol. 111, 2014, pp. 2453–2458.

[8] Ajdari, A., B. H. Jahromi, J. Papadopoulos, H. Nayeb-Hashemi, and A. Vaziri. Hierarchical honeycombs with tailorable properties. *International Journal of Solids and Structures*, Vol. 49, 2012, pp. 1413–1419.

[9] Montemurro, M., G. Bertolino, and T. Roiné. A general multi-scale topology optimisation method for lightweight lattice structures obtained through additive manufacturing technology. *Composite Structures*, Vol. 258, 2021, id. 113360.

[10] Compton, B. G. and J. A. Lewis. 3D-printing of lightweight cellular composites. *Advanced Materials*, Vol. 26, 2014, pp. 5930–5935.

[11] Estakhrianhaghighi, E., A. Mirabolghasemi, Y. Zhang, L. Lessard, and A. Akbarzadeh. 3D-printed wood-fiber reinforced architected cellular composites. *Advanced Engineering Materials*, Vol. 22, 2020, id. 2000565.

[12] Ajdari, A., H. Nayeb-Hashemi, and A. Vaziri. Dynamic crushing and energy absorption of regular, irregular and functionally graded cellular structures. *International Journal of Solids and Structures*, Vol. 48, 2011, pp. 506–516.

[13] Zhang, J., H. Wei, Z. Wang, and L. Zhao. Dynamic crushing of uniform and density graded cellular structures based on the

circle arc model. *Latin American Journal of Solids and Structures*, Vol. 12, 2015, pp. 1102–1125.

[14] Liu, Y., H. X. Wu, and B. Wang. Gradient design of metal hollow sphere (MHS) foams with density gradients. *Composites Part B: Engineering*, Vol. 43, 2012, pp. 1346–1352.

[15] Chen, J., P. Zhang, Y. Cheng, and J. Liu. On the crushing response of the functionally graded metallic foams based on 3D Voronoi model. *Thin-Walled Structures*, Vol. 157, 2020, id. 107085.

[16] Zhang, J., Z. Wang, and L. Zhao. Dynamic response of functionally graded cellular materials based on the Voronoi model. *Composites Part B: Engineering*, Vol. 85, 2016, pp. 176–187.

[17] Liang, M., Z. Li, F. Lu, and X. Li. Theoretical and numerical investigation of blast responses of continuous-density graded cellular materials. *Composite Structures*, Vol. 164, 2017, pp. 170–179.

[18] Chen, D., S. Kitipornchai, and J. Yang. Dynamic response and energy absorption of functionally graded porous structures. *Materials and Design*, Vol. 140, 2018, pp. 473–487.

[19] Lan, X. K., Q. Huang, T. Zhou, and S. S. Feng. Dynamic response of gradient cellular materials under high velocity impact. *IOP Conference Series: Materials Science and Engineering*, Vol. 629, 2019, id. 012036.

[20] Duan, Y., X. Zhao, Z. Liu, N. Hou, H. Liu, B. Du, et al. Dynamic response of additively manufactured graded foams. *Composites Part B: Engineering*, Vol. 183, 2020, id. 107630.

[21] Duan, Y., Y. Ding, Z. Liu, N. Hou, X. Zhao, H. Liu, et al. Effects of cell size vs. cell-wall thickness gradients on compressive behavior of additively manufactured foams. *Composites Science and Technology*, Vol. 199, 2020, id. 108339.

[22] Liu, H. and B. F. Ng. Dynamic response of density-graded foam subjected to soft impact. *Composite Structures*, Vol. 284, 2022, id. 115145.

[23] Zhao, H., Y. Han, C. Pan, D. Yang, H. Wang, X. Zeng, et al. Design and mechanical properties verification of gradient Voronoi scaffold for bone tissue engineering. *Micromachines*, Vol. 12, 2021, id. 664.

[24] Reid, S. R. and C. Peng. Dynamic uniaxial crushing of wood. *International Journal of Impact Engineering*, Vol. 19, 1997, pp. 531–570.

[25] Lopatnikov, S. L., B. A. Gama, M. J. Haque, C. Krauthauser, J. W. Gillespie, M. Guden, et al. Dynamics of metal foam deformation during Taylor cylinder – Hopkinson bar impact experiment. *Composite Structures*, Vol. 61, 2003, pp. 61–71.

[26] Zheng, Z., Y. Liu, J. Yu, and S. R. Reid. Dynamic crushing of cellular materials: continuum-based wave models for the transitional and shock modes. *International Journal of Impact Engineering*, Vol. 42, 2012, pp. 66–79.

[27] Zheng, Z., C. Wang, J. Yu, S. R. Reid, and J. J. Harrigan. Dynamic stress–strain states for metal foams using a 3D cellular model. *Journal of the Mechanics and Physics of Solids*, Vol. 72, 2014, pp. 93–114.

[28] Shen, C. J., T. X. Yu, and G. Lu. Double shock mode in graded cellular rod under impact. *International Journal of Solids and Structures*, Vol. 50, 2013, pp. 217–233.

[29] Karagiozova, D. and M. Alves. Propagation of compaction waves in cellular materials with continuously varying density. *International Journal of Solids and Structures*, Vol. 71, 2015, pp. 323–337.

[30] Liu, J., B. Hou, F. Lu, and H. Zhao. A theoretical study of shock front propagation in the density graded cellular rods. *International Journal of Impact Engineering*, Vol. 80, 2015, pp. 133–142.

[31] Yang, J., S. Wang, Y. Ding, Z. Zheng, and J. Yu. Crashworthiness of graded cellular materials: a design strategy based on a nonlinear plastic shock model. *Materials Science and Engineering: A*, Vol. 680, 2017, pp. 411–420.

[32] Ding, Y., Z. Zheng, Y. Wang, and F. Zhou. Impact resistance and design of graded cellular cladding. *International Journal of Applied Mechanics*, Vol. 10, 2018, id. 1850107.

[33] Liu, H., S. Ding, and B. F. Ng. Impact response and energy absorption of functionally graded foam under temperature gradient environment. *Composites Part B: Engineering*, Vol. 172, 2019, pp. 516–532.

[34] Tran, P., T. D. Ngo, A. Ghazlan, and D. Hui. Bimaterial 3D printing and numerical analysis of bio-inspired composite structures under in-plane and transverse loadings. *Composites Part B: Engineering*, Vol. 108, 2017, pp. 210–223.

[35] Gu, Y. and X. Xu. Novel gradient design and simulation of Voronoi structures. *International Journal of Applied Mechanics*, Vol. 10, 2018, id. 1850079.

[36] Papka, S. D. and S. Kyriakides. In-plane compressive response and crushing of honeycomb. *Journal of the Mechanics and Physics of Solids*, Vol. 42, 1994, pp. 1499–1532.

[37] Gibson, L. J. and M. F. Ashby. *Cellular solids: structure and properties*, Press Syndicate of the University of Cambridge, Cambridge, UK, 1997.

[38] Li, Q. M., I. Magkiriadis, and J. J. Harrigan. Compressive strain at the onset of densification of cellular solids. *Journal of Cellular Plastics*, Vol. 42, 2006, pp. 371–392.

[39] Liu, Y. D., J. L. Yu, Z. J. Zheng, and J. R. Li. A numerical study on the rate sensitivity of cellular metals. *International Journal of Solids and Structures*, Vol. 46, 2009, pp. 3988–3998.